

Seismic Wave Scattering Through a Compressed Hybrid BEM/FEM Method.

Nicolás Guarín-Zapata, Juan Gomez and Juan Jaramillo

Departamento de Ingeniería Civil

Universidad EAFIT

Medellín,

Colombia

jgomezc1@eafit.edu.co

March 1, 2022

Abstract

Approximate numerical techniques, for the solution of the elastic wave scattering problem over semi-infinite domains are reviewed. The approximations involve the representation of the half-space by a boundary condition described in terms of 2D boundary element discretizations. The classical BEM matrices are initially re-written into the form of a dense dynamic stiffness matrix and later approximated to a banded matrix. The resulting final banded matrix is then used like a standard finite element to solve the wave scattering problem at lower memory requirements. The accuracy of the reviewed methods is benchmarked against the classical problems of a semi-circular and a rectangular canyon. Results are presented in the time and frequency domain, as well as in terms of relative errors in the considered approximations. The main goal of the paper is to give the analyst a method that can be used at the practising level where an approximate solution is enough in order to support engineering decisions.

Keywords: Wave scattering, boundary element method, finite element method, hybrid BEM/FEM.

1 Introduction

One of the main challenges in the numerical simulation of wave scattering problems, over infinite or semi-infinite domains, is the proper imposition of radiation boundary conditions: When

the analysis is performed using a full domain method, e.g., the finite differences method (FDM) or the finite element method (FEM), one has to render finite the computational domain, and use artificial boundary elements to approximate radiation damping. A wide variety of absorbing boundary elements are available in the literature, (Lysmer & Kuhlemeyer, 1969; Engquist & Majda, 1977; Clayton & Engquist, 1977). Most of these elements suffer deficiencies, like dependence of the performance on the angle of the incident wave or a limited frequency band of efficient operation. On the other hand, among the many techniques available to approximate Sommerfeld’s radiation boundary conditions, those based on integral formulations are the most accurate (Pao & Varatharajulu, 1976; Banerjee, 1994a; Sánchez-Sesma et al., 1993); although their coupling to existing finite element codes introduces inconvenient features, since their resulting coefficient matrices are asymmetric and fully populated and destroy many of the appealing features of finite element methods. In this work we explore approximations to the radiation boundary condition, that combine the accuracy of integral-based formulations with the advantages of the finite element algorithm. Our approximate representation is intended to be useful in the solution of scattering problems of moderate size using existing finite element codes and the resources available in current personal computers.

In general, the complexity of a formulation to approximate the radiation boundary condition is a function of the degree of space-time non-locality introduced in the boundary model. In the case of classical FDs and FEs, non-locality is an unnatural condition: Consequently, in order to obtain effective solutions, the analyst must sacrifice accuracy at the expense of non-locality; with accurate results obtained after a trade-off between non-locality and the use of Saint-Venant-end-effects leading to large computational models. One of the first contributions in absorbing boundaries, but still one of the most popular ones, is the fully-local, viscous boundary element by Lysmer & Kuhlemeyer (1969). This boundary provides the conceptual basis of most of the currently used elements, which exhibit various levels of efficiency with increasing levels of non-locality, (Berenger, 1994; Soudkhah & Pak, 2012; Lee et al., 2012; Zheng et al., 2013; Duru & Kreiss, 2012). Moreover, many of these absorbing conditions have been used in recent FDs and FEs simulations of seismic regions, as large as the state of California and for frequencies up to 4.0 Hz, (Frankel, 1993; Komatitsch & Tromp, 1999; Min et al., 2003; Bielak et al., 2003; Komatitsch et al., 2004; Givoli, 2004; Frehner et al., 2008; Ichimura et al., 2009; Lee et al., 2009a,b, 2010; Bielak et al., 2010; Chaljub et al., 2010; Lan & Zhang, 2011). In a second class of methods, which are inherently non-local in space and time, (Pao & Varatharajulu, 1976; Manolis & Beskos, 1988; Sánchez-Sesma & Campillo, 1991; Banerjee, 1994a; Sánchez-Sesma & Luzón, 1995; Janod & Coutant, 2000; Iturrarán-Viveros et al., 2005), the radiation condition is imposed through fully coupled boundary integral formulations: In those cases the half-space condition is analytically satisfied by the Green’s function, but the resulting algorithm, although highly accurate is also computationally demanding with coefficient matrices which are non-symmetric and fully populated.

A third solution strategy that has been popular during many years, is a combination that approximates radiation damping via the BEM technique, while the scatterer, (including heterogeneities and/or nonlinearities), is treated with an FEM algorithm (Brebbia & Georgiou, 1979; Beer & Meek, 1981; Banerjee, 1994b; Zienkiewicz et al., 1977; Zienkiewicz & Taylor, 2005; Boutchicha et al., 2007; Helledorfer et al., 2008; Seghir et al., 2009; Bielak et al., 2009). That approach becomes

especially attractive when the BEM discretization is written in the form of a displacements-based finite element, representing the semi-infinite domain as a half-space-super-element (HSSE) and favouring its straightforward coupling to a finite element model for the scatterer. Although the coupling of BEM and FEM algorithms can be accomplished in a wide majority of commercially available finite element codes that assimilate user element subroutines, e.g., ([Abaqus, 1989](#); [Taylor, 2011](#)), the asymmetric and dense character of the HSSE-coefficient-matrix still restrains the advantages of the finite element method. Therefore, additional modifications must be imposed to the resulting radiation boundary approximation, in order to obtain an efficient and accurate formulation that preserves the nice properties of the finite element method. In this work we enforce the HSSE-coefficient-matrix to remain banded and symmetric, and assess the effect upon the solution accuracy of such compression scheme.

Compression schemes for the boundary element matrices have been used in the past, but all of them performed the matrix compression at the boundary element level, i.e. in the discrete versions of the displacements and traction kernels. For instance, [Bouchon et al. \(1995\)](#) used the criteria of making zero each term of the traction and displacement matrices, where an original absolute value below a preselected threshold was identified; [Ostrowski et al. \(2006\)](#) used hierarchical matrices and adaptive cross approximation, which is a purely algebraic method, to compress the discrete BEM integral operators; [Abe et al. \(2001\)](#) and [Eppler & Harbrecht \(2005\)](#) used a wavelet BEM technique to achieve the packing of the resulting matrices. The fast multi-poles boundary element methods (FM-BEM) introduced by [Liu \(2009\)](#), have gained popularity due to its low computational cost in both, storage requirements and CPU time; these methods are based on a far field expansion of the kernels of the integral equations. In this work, we follow a slightly different approach since we directly operate in the final resulting BEM dynamic stiffness matrix; this operation is a mandatory requirement if the goal is to preserve the advantages of the classical displacement-based finite element method. Such requirement is clarified if one considers the fact that the inverse of a banded matrix is not generally banded, and although the product of banded matrices is still banded, the resulting half-band-width is larger than in the original single matrices.

In the current work we first review the well-known direct and indirect BEM algorithms, and establish the connection between the final HSSE matrices obtained with both methods. The resulting matrices are then compressed using (i) a threshold criteria and (ii) a method based on the distance to the diagonal of the different terms; this method is termed herein a half-band-width-method. The resulting HSSEs are coupled into an existing finite element code and tested in the solution of two well documented scattering problems, namely a semicircular and a rectangular canyon. Both problems are rich in scattered motions and contain different sources of diffraction: As shown by different authors ([Bielak & Christiano, 1984](#); [Jaramillo et al., 2013](#)) the scattered and diffracted parts of the total field contain the motions that must be absorbed by the HSSE. The article is organized as follows: The first part summarizes the scattering problem in terms of integral equations, leading to boundary element algorithms and the formulation of the HSSE coefficient matrices, together with its coupling to existing finite element codes. We then discuss and apply the compression criteria to the solution of both canyons. The results, which are shown in the frequency and time domain are then compared in terms of transfer functions and synthetic seismograms along the canyon surfaces.

2 Solution of the Scattering Problem

2.1 Direct and Indirect BEM Formulation and coupling to the finite element method

The general scattering problem is schematized in fig. 1. Since the scatterer is treated with a classical FEM algorithm, we only discuss the formulation of the boundary value problem for the half-space part of the domain. In this work we use a method due to [Bielak & Christiano \(1984\)](#) where the only unknown in the half-space corresponds to the scattered field. In this way, the external plane wave excitation is converted into an equivalent system of internal sources, located along the contact interface between the two media. The problem is then formulated in terms of the Green's function using either an integral representation theorem or a plain superposition of sources.

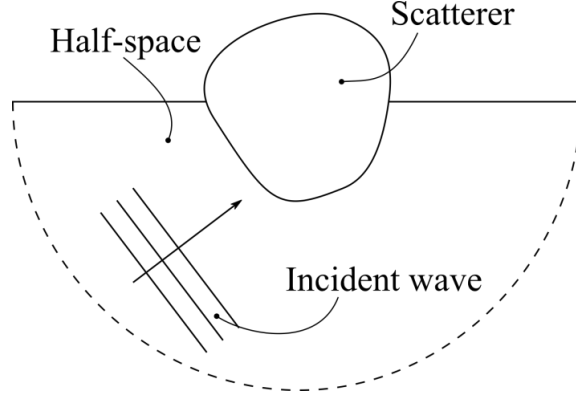


Figure 1: Schematic representation of the scattering problem.

Regardless of whether a direct or indirect BEM approach is used, both methods find their basic foundation in the concept of the fundamental solution or the specific problem Green's functions $G_{ij}(\vec{x}, \vec{\xi})$ and $H_{ij}(\vec{x}, \vec{\xi}, \hat{n}_x)$. These functions allow us to express respectively the i -th displacement u_i and traction components t_i at a field point \vec{x} due to a load P_j applied in the j -th direction at a point $\vec{\xi}$ according to eq. (1);

$$\begin{aligned} u_i(\vec{x}) &= G_{ij}(\vec{x}, \vec{\xi}) P_j(\vec{\xi}) \\ t_i(\vec{x}, \hat{n}_x) &= H_{ij}(\vec{x}, \vec{\xi}, \hat{n}_x) P_j(\vec{\xi}). \end{aligned} \tag{1}$$

and where it is clear that $H_{ij}(\vec{x}, \vec{\xi}, \hat{n}_x)$ is the tractions counterpart of the displacement Green's function $G_{ij}(\vec{x}, \vec{\xi})$. In the above \hat{n}_x denotes the normal vector outward to the surface at a field

point \vec{x} . Direct use of eq. (1) into Betti's reciprocity theorem for the scattered and the fundamental states, yields Somigliana identity which is the basis of the integral equation to be solved in a direct boundary element method as given in eq. (2)

$$C_{ij}(\vec{\xi})u_i(\vec{\xi}) = \int_S G_{ij}(\vec{x}, \vec{\xi})t_i(\vec{x}, \hat{n}_x) dS(\vec{x}) - \int_S H_{ij}(\vec{x}, \hat{n}_x; \vec{\xi}, \hat{n}_\xi)u_i(\vec{x}) dS(\vec{x}). \quad (2)$$

where again \hat{n}_x is the surface outward normal unit vector; C_{ij} is a coefficient that depends on the smoothness of the boundary; u_i and t_i are the boundary displacements and tractions vectors respectively. Similarly, direct application of eq. (1) after assuming that the solution field is produced by an arbitrary distribution of source densities $\phi_j(\vec{\xi})$, along the boundary of the considered domain, yields the fundamental equations to be solved in an indirect boundary element method, eq. (3);

$$\begin{aligned} u_i(\vec{x}) &= \int_S G_{ij}(\vec{x}, \vec{\xi})\phi_j(\vec{\xi}) dS(\vec{\xi}) \\ t_i(\vec{x}, \hat{n}_x) &= \frac{1}{2}\phi_j(\vec{x}) + \int_S H_{ij}(\vec{x}, \vec{\xi}, \hat{n}_\xi)\phi_j(\vec{\xi}) dS(\vec{\xi}) \end{aligned} \quad (3)$$

and where the problem is now solved in a two step algorithm, where one has to find the distribution of source densities $\phi_j(\vec{\xi})$ that solves the specified boundary conditions and then finds the solution field anywhere inside the domain.

The corresponding system of algebraic equations in either case can be obtained after discretization of the field and the boundary into N (constant) elements. In the case of the direct BEM approach an algebraic equation is generated after selecting an observation point $\vec{\xi}^l$ and performing collocation along the N nodal points \vec{x}^k leading to;

$$C_{ij}U_i^l = G_{ij}^{kl}t_i^k - H_{ij}^{kl}U_i^k. \quad (4)$$

In eq. (4) the terms G_{ij}^{kl} and H_{ij}^{kl} correspond to the integrals of the Green's functions over the \vec{x}^k -element and evaluated at the $\vec{\xi}^l$ collocation point. Similarly, in the case of the indirect algorithm we generate an algebraic equation after selecting an observation point \vec{x}^k and performing collocation along the $\vec{\xi}^l$ nodal points leading to;

$$\begin{aligned} U_i^k &= \tilde{G}_{ij}^{kl}\phi_j^l \\ t_i^k &= \tilde{H}_{ij}^{kl}\phi_j^l \end{aligned} \quad (5)$$

In eq. (5) the terms \tilde{G}_{ij}^{kl} and \tilde{H}_{ij}^{kl} have the same meaning as in the direct algorithm, however, it should be noticed that the observation and field points are now reversed. Observe also that the displacement matrices G_{ij}^{kl} and \tilde{G}_{ij}^{kl} are the same in both methods because of the symmetries in the Green's function. On the contrary, the traction matrices have both directional and evaluation arguments which are transposed. The corresponding collocation scheme in each case is described in fig. 2.

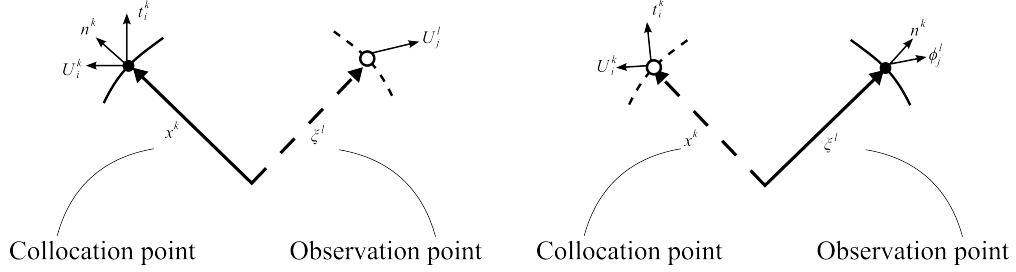


Figure 2: Definition of the observation and collocation points in the direct (left) and indirect (right) boundary element algorithms.

The problem of coupling the BEM and FEM discretizations, reduces now to the simple exercise of writing the BEM equations—relating unknown nodal tractions and displacements to prescribed nodal tractions and displacements—into the equivalent form of a nodal forces-displacements relationship like in a standard displacements based finite element method formulation. Moreover, in the case of the discussed wave propagation problem, formulated in terms of the scattered field over the half-space and when the used Green's functions are those of a semi-infinite medium, the problem simplifies even more, since there are no remote forces originating at the far surface of the BEM domain, labeled S_M in fig. 3, to be carried over to the FEM domain.

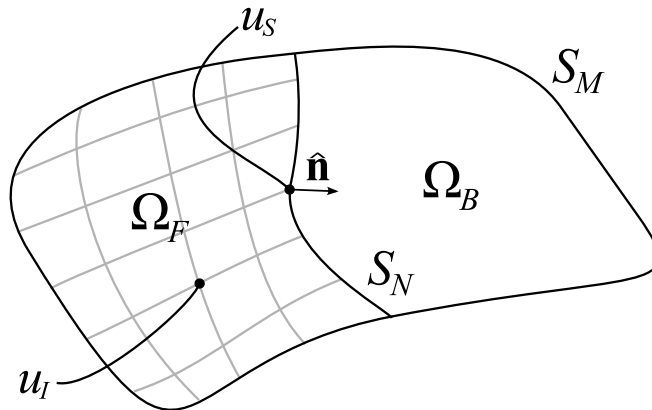


Figure 3: Schematic description of the coupling between a BEM and a FEM discretization.

In the case of plane wave incidence, the stiffness relation to be coupled and directly implemented into an existing FEM code, reduces to the Half-Space-Super-Element (HSSE) stiffness matrix and

its associated loads vector containing the incoming field, but expressed in terms of consistent nodal forces, see Bielak and Christiano (1984). Referring again to fig. 3, we let the finite element part of the domain be Ω_F . This domain is assumed to have been discretized into internal degrees of freedom U_I and the contact surface into degrees of freedom U_S . In general, we will assume that the discretizations of the BEM and the FEM meshes have different number of nodes and therefore compatibility must be enforced through displacement and coupling matrices R_u and R_t (Tassoulas, 1988), as specified in eq. (6);

$$\begin{aligned} U_N &= R_u U_S \\ F_N(\hat{n}^*) &= R_t t_S(\hat{n}) \end{aligned} \quad (6)$$

and where the normal vectors satisfy $\hat{n} = -\hat{n}^*$. Now, we can write the discrete finite element equations corresponding to the scatterer like;

$$\begin{bmatrix} K_{II} & K_{IS} \\ K_{SI} & K_{SS} \end{bmatrix} \begin{bmatrix} U_I \\ U_S \end{bmatrix} = \begin{bmatrix} F_I \\ F_S(\hat{n}) \end{bmatrix} \quad (7)$$

where $F_S(\hat{n})$ are the consistent nodal forces along the contact surface. Similarly the equations for the half-space, after having converted the BEM system into a generalized force displacement relationship are written like;

$$F_N^S(\hat{n}^*) = K_{HS} U_S^S \quad (8)$$

and where the forces along the contact surface have been denoted like $F_N^S(\hat{n}^*)$. Coupling of eq. (7) and eq. (8) using the conditions along the contact surface between displacements and forces involving the incoming field represented by the discrete terms U_S^0 and $F_S^0(\hat{n}^*)$ and given by;

$$\begin{aligned} U_S &= U_S^S + U_S^0 \\ F_S(\hat{n}) + F_S^S(\hat{n}^*) + F_S^0(\hat{n}^*) &= 0 \end{aligned} \quad (9)$$

yields;

$$\begin{bmatrix} K_{II} & K_{IS} \\ K_{SI} & K_{SS} + K_{HS} \end{bmatrix} \begin{bmatrix} U_I \\ U_S \end{bmatrix} = \begin{bmatrix} F_I \\ -F_S^0(\hat{n}^*) + K_{HS} U_S^0 \end{bmatrix} \quad (10)$$

In eq. (10) the terms U_S^0 and $F_S^0(\hat{n}^*)$ represent the incoming field in terms of displacements and forces, evaluated at the contact surface and K_{HS} describes the half-space contribution to the

global equilibrium equations. Denoting the Green tractions matrix for the direct boundary element and indirect boundary element method like H^{BEM} and H^{IBEM} respectively, yields after direct comparison of the resulting stiffness matrices the following connection between both algorithms

$$\begin{aligned} K_{HS}^{BEM} &= R_t H^{BEM} G^{-1} R_u \\ K_{HS}^{IBEM} &= R_t G^{-1} H^{IBEM} R_u \end{aligned} \quad (11)$$

2.2 Compression of the stiffness matrix

The non-local nature of the BEM matrices G and H in eq. (11), results in a finite element system of equations with a dense coefficient matrix. This result, associated to the non-local nature of the half-space superelement, is disadvantageous for its coupling in a finite element algorithm since the HSSE now controls the memory requirements and avoids the use of available and robust iterative solvers based on banded stiffness matrices. In this work we used two compression methods to impose a banded condition in the *HSSE* stiffness matrix, so we can increase computer resources and take advantage of iterative solvers available in most commercial codes. Although several works have been performed related to compression of BEM equations, we directly operate here on the resulting stiffness matrix. To the best of our knowledge a study of how this manipulation affects accuracy has not been developed. Two compression methods were used and defined as follows:

- A threshold method, where all the terms smaller than a preselected percentage of the maximum absolute value present in the original matrix are made zero
- A half-band-width method, where all the values located outside of a preselected distance from the diagonal are eliminated.

Both methods are based on the tendency of the BEM matrices to be diagonally dominant due to the singularities in the Green's functions. The threshold criteria however, is convenient as it can be applied with a sound physical basis, since the terms in the BEM matrices can be understood like influence coefficients indicating how strong is the effect of a given source in the response at a given nodal point; therefore the preselected threshold value is in fact a source intensity coefficient. The trend of the matrices to be diagonally dominant can be observed in fig. 4, where we plotted the appearance of the reduced BEM stiffness matrices for the model of a semi-circular canyon after applying the threshold criteria. The BEM stiffness matrix can be computed and compressed inside a user element subroutine, coupled to an existing finite element code. It suffices to specify the nodal points conforming the contact surface S_M and the subroutine must return the elemental contribution (see eq. (10) and eq. (11)). If the problem is directly solved in the time domain, it suffices to implement a user element subroutine UEL where the element contribution to the global system is either one of the K 's specified in eq. (11) and the contribution to the loads vector is the one appearing in eq. (10). On the other hand, if the analysis is performed in the frequency domain, where the K 's are complex valued, one needs to assume that the model has real and imaginary degrees of freedom at each node, thus doubling the number of degrees of freedom with respect to

the ones used in a direct time domain analysis. With this assumption at hand, the implementation of the finite element proceeds exactly like in the time domain. For instance, such a generalized framework has been proposed by Mosquera (2013).

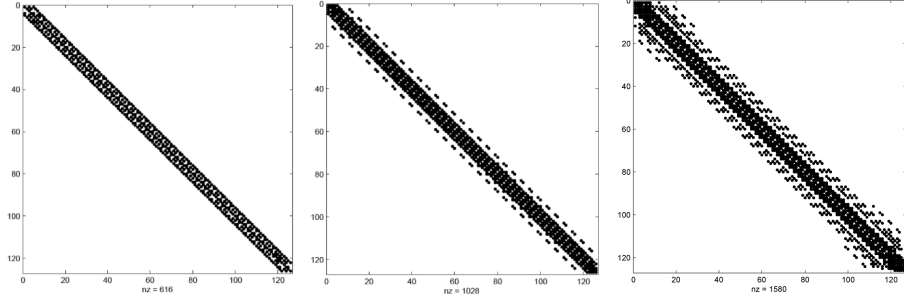


Figure 4: Appearance of the stiffness matrices for a semicircular canyon after applying the threshold criteria with values (a) 0.01 (less accurate), (b) 0.001 and (c) 0.0001 (more accurate).

3 Results

3.1 Compressed Stiffness Matrix Formulation

The well known benchmark problems of a semi-circular and a rectangular canyon were selected in order to test and evaluate the loss of accuracy of the stiffness matrix approximation. These problems constitute a worst case scenario for the approximation if the resulting matrices are interpreted like absorbing boundaries. The response of both canyons to P and SV waves incident at 0° and 30° with respect to the vertical was calculated. For the excitation we applied an incoming field corresponding to a Ricker pulse. As a threshold value we applied a variation from 0.0 to 0.01, with 0.0 corresponding to the original complete matrix and with a larger value representing a less accurate approximation. In the case of the band-width criteria the size of the relative half-band width was varied from 0.03 to 1.0 with the complete matrix corresponding to a value of 1.0 and a null value to a matrix with only the diagonal terms. The values of the relative half-band width for matrices approximated with the threshold criteria are shown in table 1.

| Threshold | Relative half-bandwidth | | Relative storage | |
|-----------|-------------------------|-------------|------------------|-------------|
| | Semicircular | Rectangular | Semicircular | Rectangular |
| 0 | 1 | 1 | 100% | 100% |
| 10^{-5} | 0.26 | 0.25 | 45.2% | 43.8% |
| 10^{-4} | 0.13 | 0.09 | 24.3% | 17.2% |
| 10^{-3} | 0.06 | 0.05 | 11.6% | 9.8% |
| 10^{-2} | 0.03 | 0.02 | 5.9% | 4.0% |

Table 1: Relative half-band-width for the dynamic matrices compressed by the threshold criteria. Relative storage values are also presented –storing just the terms in the band.

After imposing the banded condition we are interested in determining the storage requirements for the new resultant matrix. The original needs corresponding to the full matrix requires n^2 memory words. For the new approximated matrix and storing just the terms in the band, the relative needed storage requirement, Rst , can be approximated after neglecting the words required to store the diagonal itself like;

$$Rst(Rhbw) = 2Rhbw - Rhbw^2 \quad (12)$$

and where $Rhbw$ is the relative half-band width. A storage requirement corresponding to 50% of the full matrix is equivalent to a relative half-band width of 0.3, while 0.13 would be equivalent to 25% of the original storage requirement.

Figures 5 to 12 show the transfer functions and synthetic displacement time-histories (synthetic seismograms) for a dimensionless frequency $\eta = \omega L / \pi \beta = 1.0$ where ω is the circular frequency, β the shear wave velocity and L is the characteristic canyon dimension for different cases. On the other hand we show in fig. 13 the relative errors with respect to the square-norm for different levels of approximation and for all considered incident waves. In general, the best results were obtained for the vertical displacements under P -wave incidence and for the horizontal displacements in the case of SV -wave incidence. At the same time, as was originally expected better results are obtained for the semi-circular canyon which contains less diffraction sources as compared to the rectangular canyon. This behaviour is observed for both the threshold and half-band-width criteria.

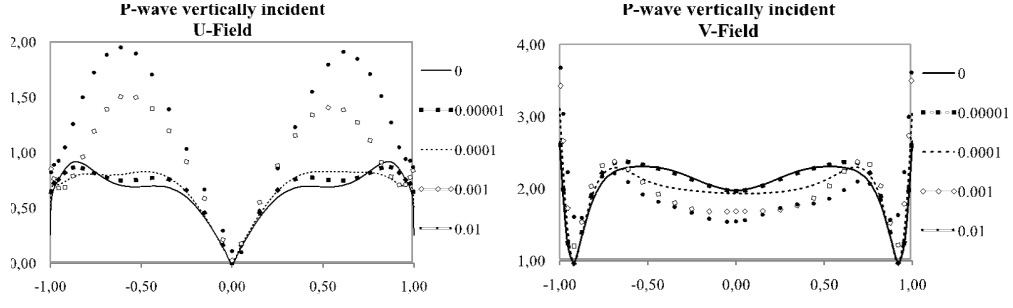


Figure 5: Transfer function for a semicircular canyon for a vertically incident P wave at a dimensionless frequency of 1.

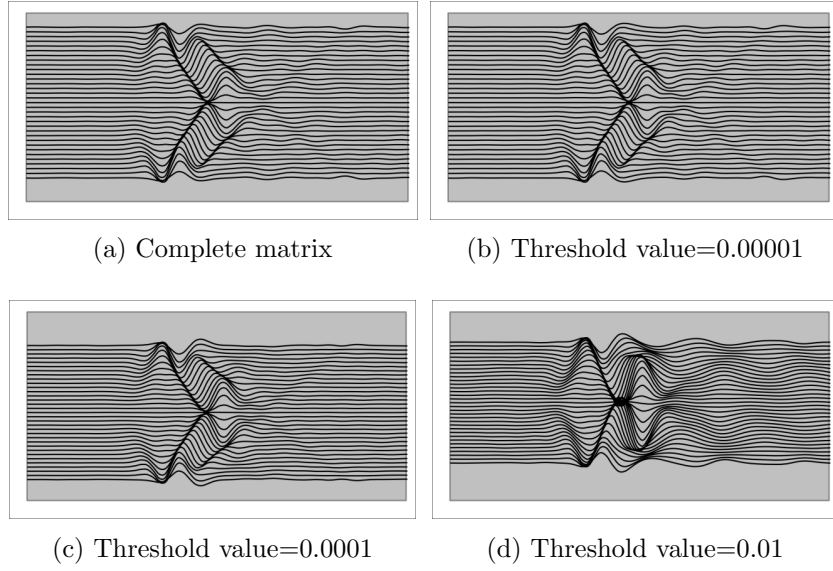


Figure 6: Synthetic seismograms for horizontal displacement for a semicircular canyon for a vertically incident P wave for different threshold values.

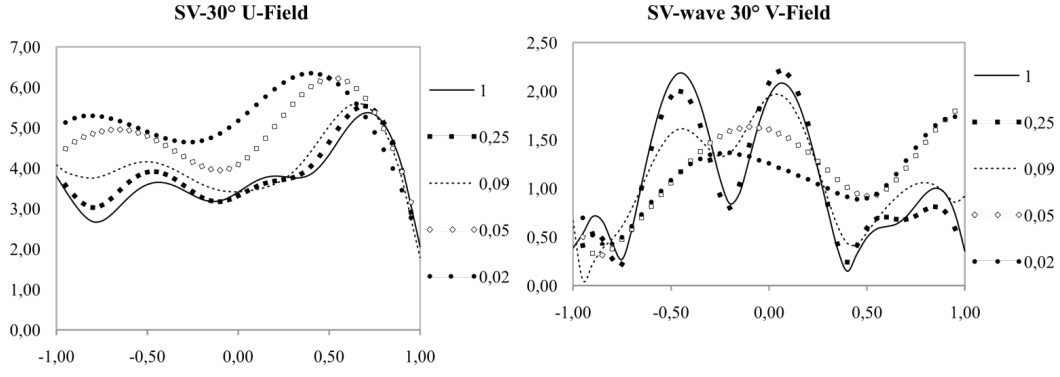


Figure 7: Transfer function for a rectangular canyon for a 30° incident SV wave at a dimensionless frequency of 1.

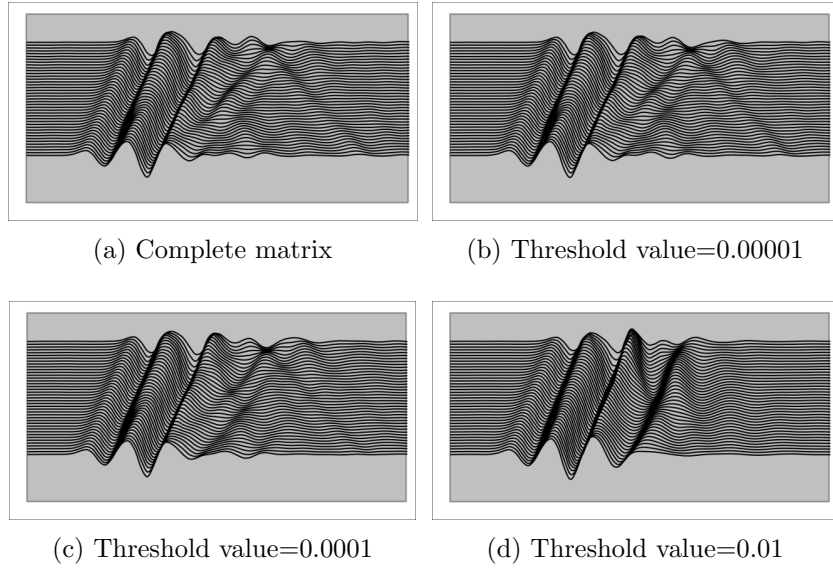


Figure 8: Synthetic seismograms for horizontal displacement for a rectangular canyon for a vertically incident SV wave for different threshold values.

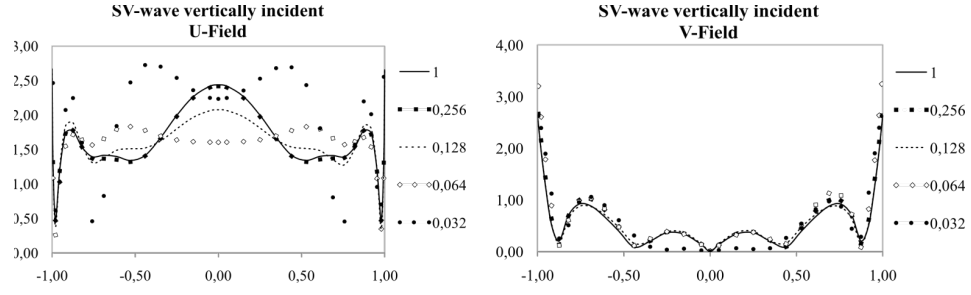


Figure 9: Transfer function for a semicircular canyon for a vertically incident SV wave at a dimensionless frequency of 1.

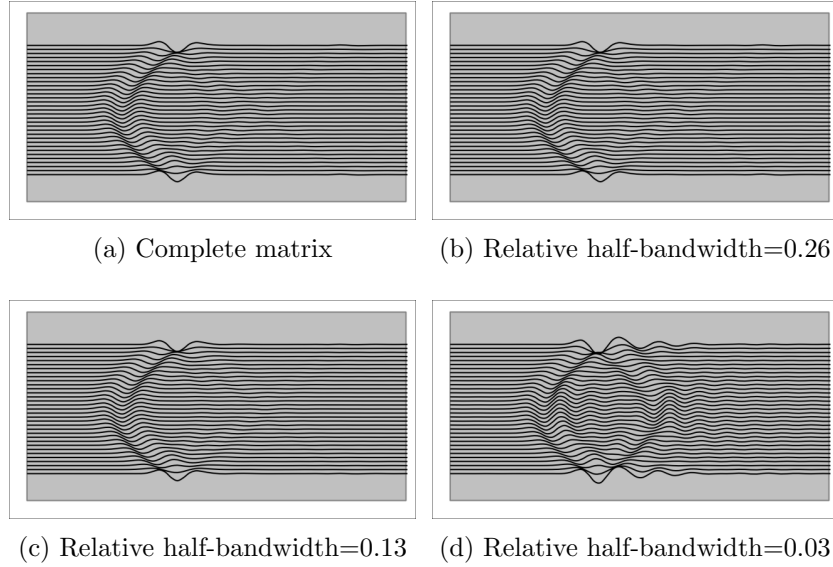


Figure 10: Synthetic seismograms for horizontal displacement for a semicircular canyon for vertically incident SV wave different half-bandwidth values.

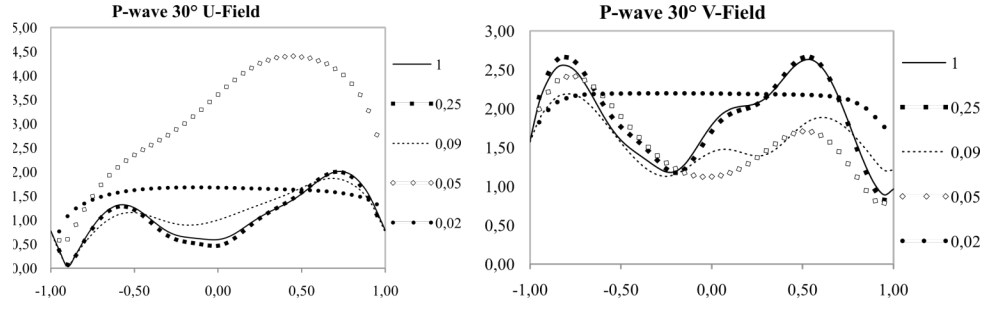


Figure 11: Transfer function for a rectangular canyon for a 30° incident P wave at a dimensionless frequency of 1.

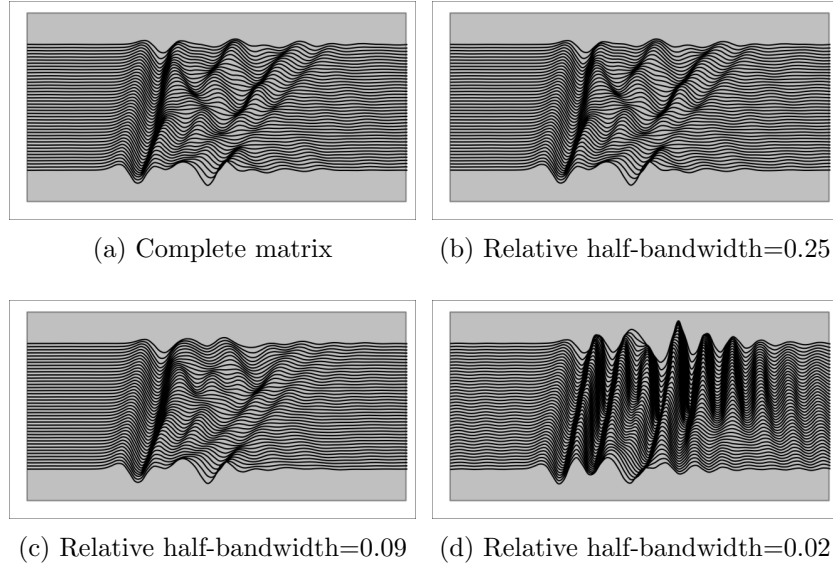


Figure 12: Synthetic seismograms for horizontal displacement for a semicircular canyon for a 30° incident P wave for different half-bandwidth values.

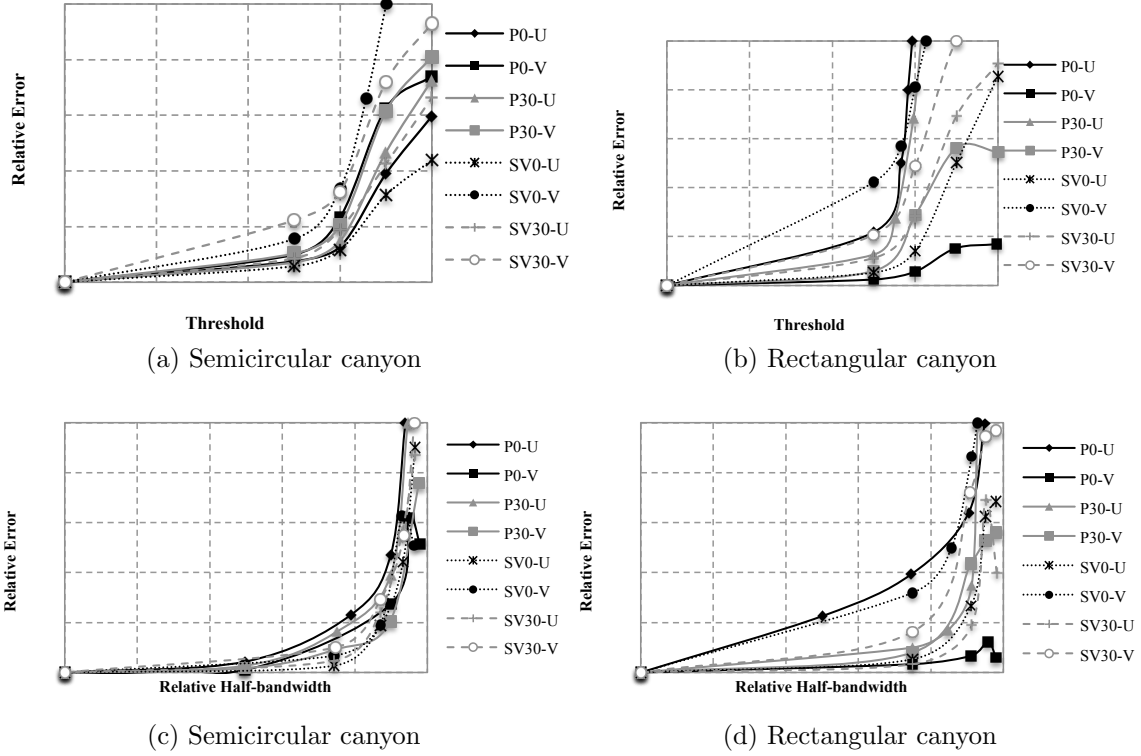


Figure 13: Comparison for different matrix compression criteria: a), b) for Threshold criterion and c), d) for Half-bandwidth criterion. In all the cases the geometry and the incidence type of wave SV or P and angle is varied for well known cases. The error is computed for the transfer function at a dimensionless frequency of 1.

4 Conclusions and Furtherwork

Two approximate numerical solution methods for the elastic wave scattering problem, were discussed and evaluated in order to facilitate the study of dispersion problems at the practising engineering level in available personal computers and within existing finite element architectures. First, the loss of accuracy associated with two different ways of converting fully dense stiffness matrices into banded stiffness matrix was evaluated. The original stiffness matrix appeared after the discretization of a half-space sub-domain with two different boundary element algorithms, e.g., a direct boundary element method and an indirect boundary element method. The proposed techniques are oriented to the solution of the problem at the engineering practising level since one arrives to a stiffness matrix that can be coupled into existing commercial finite element codes, e.g., ABAQUS and FEAP. The compression procedure results in savings in memory requirements. Although similar procedures have been previously used in order to compress full BEM matrices, to the best of our knowledge there are no published works for the compression of coupled BEM/FEM algorithms. A good approximation is obtained for vertical displacements under P-wave incidence and horizontal displacements under SV-wave incidence. A larger error is obtained for the rectan-

gular canyon because of the presence of singularity points in the tractions field along the corners. Errors as large as 50% for the considered range of approximations were found. For an error of the order of 10% a relative half-band-width of 0.13 or equivalently, a relative storage requirement of 0.25 can be used. This is a memory saving of 75%.

Aknowledgements

This project was conducted with financial support from “Departamento Administrativo de Ciencia, Tecnología e Innovación, COLCIENCIAS” and from Universidad EAFIT.

References

- Abaqus, H., 1989. Karlsson and sorenson, *Inc.,” User’s Manual,” Version, 4.*
- Abe, K., Koro, K., & Itami, K., 2001. An h-hierarchical Galerkin BEM using Haar wavelets, *Engineering Analysis with Boundary Elements*, **25**, 581–591.
- Banerjee, P., 1994a. *The boundary element methods in engineering*, McGraw-Hill, London.
- Banerjee, P. K., 1994b. *The Boundary Element Methods in Engineering*, McGraw-Hill College, 2nd edn.
- Beer, G. & Meek, J., 1981. The coupling of boundary and finite element methods for infinite domain problems in elasticity, *Boundary element method*, **1**, 575–591.
- Berenger, J.-P., 1994. A perfectly matched layer for the absorption of electromagnetic waves, *Journal of computational physics*, **114**(2), 185–200.
- Bielak, J. & Christiano, P., 1984. On the effective seismic input for non-linear soil-structure interaction systems, *Earthquake engineering & structural dynamics*, **12**(1), 107–119.
- Bielak, J., Loukakis, K., Hisada, Y., & Yoshimura, C., 2003. Domain Reduction Method for Three-Dimensional Earthquake Modeling in Localized Regions, Part I: Theory, *Bulletin of the Seismological Society of America*, **93**, 817–824.
- Bielak, J., MacCamy, R., McGhee, D., & Barry, A., 2009. Unified Symmetric BEM-FEM for Site Effects on Ground Motion SH Waves, *Journal of Engineering Mechanics*, **117**, 2265–2285.
- Bielak, J., Graves, R., Olsen, K., Taborda, R., Ramírez-Guzmán, L., Day, S., Ely, G., Roten, D., Jordan, T., Maechling, P., Urbanic, J., Cui, Y., & Juve, G., 2010. The ShakeOut earthquake scenario: Verification of three simulation sets, *Geophysical Journal International*, **180**, 375404.

- Bouchon, M., Schultz, C. A., & Tokstz, M. N., 1995. A Fast Implementation of Boundary Integral Equation Methods to Calculate the Propagation of Seismic Waves in Laterally Varying Layered Media, *Bulletin of the Seismological Society of America*, **85**(6), 1679–1687.
- Boutchicha, D., Rahmani, O., Abdelkader, M., Sahli, A., & Belarbi, A., 2007. Merging of the indirect discrete boundary elements to the finite element analysis and its application to two dimensional elastostatics problems, *International Journal of Applied Engineering Research*, **2**, 441–452.
- Brebbia, C. & Georgiou, P., 1979. Combination of boundary and finite elements for elastostatics, *Applied Mathematical Modelling*, **3**, 212–220.
- Chaljub, E., Moczo, P., Tsuno, S., Bard, P.-Y., Kristek, J., Käser, M., Stupazzini, M., & Kristekova, M., 2010. Quantitative Comparison of Four Numerical Predictions of 3D Ground Motion in the Grenoble Valley, France, *Bulletin of the Seismological Society of America*, **100**(4), 1427–1455.
- Clayton, R. & Engquist, B., 1977. Absorbing boundary conditions for acoustic and elastic wave equations, *Bulletin of the Seismological Society of America*, **67**(6), 1529–1540.
- Duru, K. & Kreiss, G., 2012. A well-posed and discretely stable perfectly matched layer for elastic wave equations in second order formulation, *Communications in Computational Physics*, **11**(5), 1643.
- Engquist, B. & Majda, A., 1977. Absorbing boundary conditions for numerical simulation of waves, *Proceedings of the National Academy of Sciences*, **74**(5), 1765–1766.
- Eppler, K. & Harbrecht, H., 2005. Fast wavelet BEM for 3D electromagnetic shaping, *Applied Numerical Mathematics*, **54**, 537–554.
- Frankel, A., 1993. Three-dimensional simulations of ground motions in the san bernardino valley, california, for hypothetical earthquakes on the san andreas fault, *Bulletin of the Seismological Society of America*, **83**(4), 1020–1041.
- Frehner, M., Schmalholz, S., Saenger, E., & Steeb, H., 2008. Comparison of finite difference and finite element methods for simulating two-dimensional scattering of elastic waves, *Physics of the Earth and Planetary Interiors*, **171**, 112–121.
- Givoli, D., 2004. High-order local non-reflecting boundary conditions: a review, *Wave Motion*, **39**(4), 319–326.
- Guarín-Zapata, N., 2012. *Simulación Numérica de Problemas de Propagación de Ondas: Dominios Infinitos y Semi-infinitos*, Master’s thesis, Universidad EAFIT.
- Helldorfer, B., Haas, M., & Kuhn, G., 2008. Automatic coupling of a boundary element code with a commercial finite element system, *Advances in Engineering Software*, **39**, 699–709.
- Ichimura, T., Hori, M., & Bielak, J., 2009. A hybrid multiresolution meshing technique for finite element three-dimensional earthquake ground motion modelling in basins including topography, *Geophysical Journal International*, **177**, 1221–1232.

- Iturrarán-Viveros, U., Vai, R., & Sánchez-Sesma, F., 2005. Scattering of elastic waves by a 2-D crack using the Indirect Boundary Element Method (IBEM)., *Geophysical Journal International*, **162**, 927–934.
- Janod, F. & Coutant, O., 2000. Seismic response of three-dimensional topographies using a time-domain boundary element method, *Geophysical Journal International*, **142**(2), 603–614.
- Jaramillo, J., Gomez, J., Saenz, M., & Vergara, J., 2013. Analytic approximation to the scattering of antiplane shear waves by free surfaces of arbitrary shape via superposition of incident, reflected and diffracted rays, *Geophysical Journal International*, **192**(3), 1132–1143.
- Komatitsch, D. & Tromp, J., 1999. Introduction to the spectral element method for three-dimensional seismic wave propagation, *Geophysical Journal International*, **139**(3), 806–822.
- Komatitsch, D., Liu, Q., Tromp, J., Süß, P., Stidham, C., & Shaw, J. H., 2004. Simulations of Ground Motion in the Los Angeles Basin Based upon the Spectral-Element Method, *Bulletin of the Seismological Society of America*, **94**(1), 187206.
- Lan, H. & Zhang, Z., 2011. Three-Dimensional Wave-Field Simulation in Heterogeneous Transversely Isotropic Medium with Irregular Free Surface, *Bulletin of the Seismological Society of America*, **101**(3), 13541370.
- Lee, C.-H., Kihou, K., Horigane, K., Tsutsui, S., Fukuda, T., Eisaki, H., Iyo, A., Yamaguchi, H., Baron, A. Q. R., Braden, M., & Yamada, K., 2010. Effect of K Doping on Phonons in $\text{Ba}_{1-x}\text{K}_x\text{Fe}_2\text{As}_2$, *Journal of the Physical Society of Japan*, **79**, 014714.
- Lee, J. H., Kim, J. K., & Tassoulas, J. L., 2012. Dynamic analysis of foundations in a layered half-space using a consistent transmitting boundary, *Earthquake and Structures*, **3**(3-4), 203–230.
- Lee, S.-J., Chan, Y.-C., Komatitsch, D., & Tromp, B.-S. H. J., 2009a. Effects of Realistic Surface Topography on Seismic Ground Motion in the Yangminshan Region of Taiwan Based Upon the Spectral-Element Method and LiDAR DTM, *Bulletin of the Seismological Society of America*, **99**(2), 681–693.
- Lee, S.-J., Komatitsch, D., Huang, B.-S., & Tromp, J., 2009b. Effects of Topography on Seismic-Wave Propagation: An Example from Northern Taiwan, *Bulletin of the Seismological Society of America*, **99**(1), 314–325.
- Liu, Y., 2009. *Fast Multipole Boundary Element Method: Theory and Applications in Engineering*, Cambridge University Press, 1st edn.
- Lysmer, J. & Kuhlemeyer, R., 1969. Finite dynamic model for infinite media, *JOURNAL OF ENGINEERING MECHANICS-ASCE (JOURNAL OF THE ENGINEERING MECHANICS DIVISION)*, **859**, 877.
- Manolis, G. & Beskos, D., 1988. *Boundary Element Methods in Elastodynamics*, Spon Press, 1st edn.

- Min, D.-J., Shin, C., Pratt, R. G., & Yoo, H. S., 2003. Weighted-Averaging Finite-Element Method for 2D Elastic Wave Equations in the Frequency Domain, *Bulletin of the Seismological Society of America*, **93**(2), 904–921.
- Mosquera, F., 2013. *Implementation of User Element Subroutines for Frequency Domain Analysis of Wave Scattering Problems with Commercial Finite Element Codes*, Master’s thesis, Universidad EAFIT.
- Ostrowski, J., Andjelic, Z., Bebendorf, M., Cranganu-Cretu, B., & Smajic, J., 2006. Fast BEM-Solution of Laplace Problems With \mathcal{H} -Matrices and ACA, *IEEE TRANSACTIONS ON MAGNETICS*, **42**(4), 627–630.
- Pao, Y. H. & Varatharajulu, V., 1976. Huygens principle, radiation conditions, and integral formulas for the scattering of elastic waves, *The Journal of the Acoustical Society of America*, **59**(6), 1361–1371.
- Sánchez-Sesma, F. & Campillo, M., 1991. Diffraction of P, SV, and Rayleigh waves by topographic features: A boundary integral formulation, *Bulletin of the Seismological Society of America*, **81**(6), 2234–2253.
- Sánchez-Sesma, F. & Luzón, F., 1995. Seismic response of three-dimensional alluvial valleys for incident P, S and Rayleigh waves, *Bulletin of the Seismological Society of America*, **85**, 269–284.
- Sánchez-Sesma, F., Ramos-Martínez, J., & Campillo, M., 1993. An indirect boundary element method applied to simulate the seismic response of alluvial valleys for incident p, s and rayleigh waves, *Earthquake engineering & structural dynamics*, **22**(4), 279–295.
- Seghir, A., Tahakourt, A., & Bonnet, G., 2009. Coupling FEM and symmetric BEM for dynamic interaction of dam-reservoir systems, *Engineering Analysis with Boundary Elements*, **33**, 1201–1210.
- Soudkhah, M. & Pak, R., 2012. Wave absorbing-boundary method in seismic centrifuge simulation of vertical free-field ground motion, *Computers and Geotechnics*, **43**, 155–164.
- Tassoulas, J. L., 1988. Dynamic soil-structure interaction, in *Boundary element methods in structural analysis*, pp. 273–308, ASCE.
- Taylor, R., 2011. *FEAP/Programmer Manual version 8.3*, University of Berkeley.
- Zheng, Y., Huang, X., et al., 2013. Anisotropic perfectly matched layers for elastic waves in cartesian and curvilinear coordinates, Tech. rep., Massachusetts Institute of Technology. Earth Resources Laboratory.
- Zienkiewicz, O. & Taylor, R., 2005. *The Finite Element Method for Solid and Structural Mechanics*, vol. 2, Butterworth-Heinemann, 6th edn.
- Zienkiewicz, O. C., Kelly, D. W., & Bettess, P., 1977. The Coupling of the Finite Element Method and Boundary Solution Procedures, *International Journal of Numerical Methods in Engineering*, **11**(2), 355–375.